Protein-based human iPS cells efficiently generate functional dopamine neurons and can treat a rat model of Parkinson disease

Yong-Hee Rhee, … , Kwang-Soo Kim, Sang-Hun Lee

Research Article   Stem cells

Parkinson disease (PD) involves the selective loss of midbrain dopamine (mDA) neurons and is a possible target disease for stem cell–based therapy. Human induced pluripotent stem cells (hiPSCs) are a potentially unlimited source of patient-specific cells for transplantation. However, it is critical to evaluate the safety of hiPSCs generated by different reprogramming methods. Here, we compared multiple hiPSC lines derived by virus- and protein-based reprogramming to human ES cells (hESCs). Neuronal precursor cells (NPCs) and dopamine (DA) neurons delivered from lentivirus-based hiPSCs exhibited residual expression of exogenous reprogramming genes, but those cells derived from retrovirus- and protein-based hiPSCs did not. Furthermore, NPCs derived from virus-based hiPSCs exhibited early senescence and apoptotic cell death during passaging, which was preceded by abrupt induction of p53. In contrast, NPCs derived from hESCs and protein-based hiPSCs were highly expandable without senescence. DA neurons derived from protein-based hiPSCs exhibited gene expression, physiological, and electrophysiological properties similar to those of mDA neurons. Transplantation of these cells into rats with striatal lesions, a model of PD, significantly rescued motor deficits. These data support the clinical potential of protein-based hiPSCs for personalized cell therapy of PD.

Find the latest version:

https://jci.me/45794-pdf

Protein-based human iPS cells efficiently generate functional dopamine neurons and can treat a rat model of Parkinson disease

Yong-Hee Rhee,[1,2,3] Ji-Yun Ko,[1,2] Mi-Yoon Chang,[4] Sang-Hoon Yi,[1,2] Dohoon Kim,[4] Chun-Hyung Kim,[4] Jae-Won Shim,[1] A-Young Jo,[1] Byung-Woo Kim,[1,2] Hyunsu Lee,[5] Suk-Ho Lee,[5] Wonhee Suh,[6] Chang-Hwan Park,[2,3] Hyun-Chul Koh,[2,7] Yong-Sung Lee,[1,2,3] Robert Lanza,[8] Kwang-Soo Kim,[4,6] and Sang-Hun Lee[1,2]

[1]Department of Biochemistry and Molecular Biology, College of Medicine, [2]Hanyang Biomedical Research Institute, and [3]Graduate School of Biomedical and Engineering, Hanyang University, Seoul, Republic of Korea. [4]Molecular Neurobiology Laboratory, Department of Psychiatry and Harvard Stem Cell Institute, McLean Hospital/Harvard Medical School, Belmont, Massachusetts, USA. [5]Cell Physiology Laboratory, Department of Physiology, Seoul National University College of Medicine, Seoul, Republic of Korea. [6]CHA Stem Cell Institute, CHA University, Seoul, Republic of Korea. [7]Department of Pharmacology, College of Medicine, Hanyang University, Seoul, Republic of Korea. [8]Stem Cell and Regenerative Medicine International, Marlborough, Massachusetts, USA.

Parkinson disease (PD) involves the selective loss of midbrain dopamine (mDA) neurons and is a possible target disease for stem cell–based therapy. Human induced pluripotent stem cells (hiPSCs) are a potentially unlimited source of patient-specific cells for transplantation. However, it is critical to evaluate the safety of hiPSCs generated by different reprogramming methods. Here, we compared multiple hiPSC lines derived by virus- and protein-based reprogramming to human ES cells (hESCs). Neuronal precursor cells (NPCs) and dopamine (DA) neurons delivered from lentivirus-based hiPSCs exhibited residual expression of exogenous reprogramming genes, but those cells derived from retrovirus- and protein-based hiPSCs did not. Furthermore, NPCs derived from virus-based hiPSCs exhibited early senescence and apoptotic cell death during passaging, which was preceded by abrupt induction of p53. In contrast, NPCs derived from hESCs and protein-based hiPSCs were highly expandable without senescence. DA neurons derived from protein-based hiPSCs exhibited gene expression, physiological, and electrophysiological properties similar to those of mDA neurons. Transplantation of these cells into rats with striatal lesions, a model of PD, significantly rescued motor deficits. These data support the clinical potential of protein-based hiPSCs for personalized cell therapy of PD.

Introduction

Parkinson disease (PD) involves progressive loss of midbrain dopamine (mDA) neurons in the substantia nigra, leading to decreased levels of dopamine (DA) in the striatum, which causes dysfunctional movement symptoms such as bradykinesia, rigidity, and tremor (1). Available drugs offer only symptomatic relief and are associated with severe side effects such as dyskinesia. A promising alternative is cell-based transplantation therapy. Open-label transplantation trials using human fetal mesencephalic tissues have demonstrated that grafted cells can reinnervate the striatum, restore DA neurotransmission, and, in some patients, dramatically improve motor dysfunctions associated with PD, even after a decade (2). Unfortunately, fetal cell transplantation has significant ethical, technical, and practical limitations. The limited availability of fetal tissues and variable functional outcomes (3, 4) has created demand for a standardized and unlimited cell source for PD.

Since induced pluripotent stem cells (iPSCs) can be generated from patients' tissues and differentiate into all lineage cell types, they are an ideal source of cells for personalized replacement therapy (5–9). To evaluate their potential for treating human disease, it is important to assess their differentiation and cellular properties. The

majority of human iPSC (hiPSC) lines have been generated using lentiviral and retroviral methods, which are known to generate multiple chromosomal integrations and possible genetic dysfunction. To our knowledge, there have been no studies to date systematically comparing the physiological and differentiation properties of hiPSCs generated using different reprogramming methods.

To overcome the potential safety issues associated with using viruses, we recently generated the first hiPSC lines by direct delivery of 4 reprogramming proteins fused to a cell penetrating peptide (10). In the present study, we addressed whether hiPSCs generated using viral and protein reprogramming methods exhibit fundamental differences in their cellular, molecular, and differentiation properties and whether protein-based hiPSCs can efficiently generate functional mDA-like neurons.

Results

Induction of hiPSCs into primitive neuroepithelial cell types. To explore the potential of hiPSCs for cell therapy of PD, we evaluated 8 hiPSC lines (Table 1) generated by lentiviral transduction (Lenti-1–Lenti-4), retroviral transduction (Retro-1 and Retro-2), and direct delivery of arginine-tagged reprogramming proteins (Pro-1 and Pro-2). We also used human ES cell (hESC) lines H9 and HSF-6 as controls (Table 2). All 8 hiPSC lines exhibited morphological features typical of hESCs (e.g., large nucleus with prominent nucleoli; Supplemental Figure 1A; supplemental material available online with this article; doi:10.1172/JCI45794DS1) and expressed undifferentiated hESC markers such as

Table 1

hiPSC lines used

Name	Original name	Source (human)	Reprogramming factors	Method	Establishing institute	Reference
Lenti-1	IMR90-1	IMR-90	*OCT4, SOX2, NANOG, LIN28*	Lentivirus	University of Wisconsin	7
Lenti-2	IMR90-4	IMR-90	*OCT4, SOX2, NANOG, LIN28*	Lentivirus	University of Wisconsin	7
Lenti-3	Foreskin-1	Foreskin	*OCT4, SOX2, NANOG, LIN28*	Lentivirus	University of Wisconsin	7
Lenti-4	SES8	Aortic vascular smooth muscle	*OCT4, SOX2, NANOG, LIN28, KLF4*	Lentivirus	CHA Stem Cell Institute	47
Retro-1	Rv-hiPS 01-1	Newborn fibroblast	*OCT4, SOX2, KLF4, MYC*	Retrovirus	Harvard	10
Retro-2	Rv-hiPS 02-3	Newborn fibroblast	*OCT4, SOX2, KLF4, MYC*	Retrovirus	Harvard	10
Pro-1	piPSC-#1	Newborn fibroblast	*OCT4, SOX2, KLF4, MYC*	Protein	Harvard	10
Pro-2	piPSC-#2	Newborn fibroblast	*OCT4, SOX2, KLF4, MYC*	Protein	Harvard	10

Oct4, Nanog, and tumor recognition antigens 1–60 and 1–81 (Tra-1-60 and Tra-1-81, respectively; Supplemental Figure 1B and data not shown). Since individual ES cell (ESC) and iPSC lines are known to have different propensities to differentiate into specific cell lineages (11–13), we first optimized in vitro differentiation methods to generate neuronal precursor cells (NPCs) and DA neurons from these diverse hiPSC lines. Based on previous studies showing efficient neural induction and/or proliferation of NPCs on different feeder cells (14–19), we first optimized the stromal coculture method to ensure efficient neural induction from hiPSC and hESC lines. As schematized in Figure 1A, undifferentiated hiPSCs maintained on mouse embryonic fibroblasts (MEFs) were sequentially cocultured onto MS5 feeder cells and MS5 stably expressing sonic hedgehog (MS5-SHH). During this coculturing, hiPSCs and hESCs changed their morphology into compactly assembled and demarcated cells with abundant cytoplasm and then into tubular rosette-like structures abundantly expressing NPC-specific markers such as Pax6, nestin, and Sox2 (Figure 1, B, C, and G–I). Expression of cadherin 2, type1 (Cdh2; also referred to as N-cadherin) was asymmetrically localized on the luminal side of the rosettes (Figure 1, H and I), a characteristic feature of primitive neuroepithelial rosette structures (20, 21). Notably, supplementation of bFGF during the first week of coculture greatly enhanced yields of neural colony formation from certain hiPSC lines (especially Pro-1 and Pro-2; data not shown), probably by bFGF effects in increasing cell survival and neural specification of the differentiating hiPSCs (22). Using this optimized coculture method, all hiPSC and hESC lines generated primitive neural structures in greater than 50% of colonies within 3 weeks (Supplemental Figure 2A). These primitive neural colonies were harvested by mechanical dissection for the in vitro differentiation studies described below.

Generation of midbrain-type NPCs and DA neurons from hiPSCs. When neuroepithelial colonies were transferred to a fibronectin-coated (FN-coated) surface, the cells in the center of the colonies were proliferating and were positive for the NPC marker nestin and the proliferating cell marker Ki67, whereas the cells in the periphery underwent neuronal differentiation, emanating extensive neurites positive for the neuronal marker tubulin beta III (TuJ1) and the DA marker tyrosine hydroxylase (TH) (Figure 1, D, J, and K). To obtain a more homogenous NPC population, the colonies were dissociated into single cells and cultured in the presence of bFGF, a mitogen for NPCs. At the same time, SHH and FGF8 were added to induce midbrain patterning of NPCs (Figure 1A). Based on this combination of (a) elimination of differentiated and differentiating neuronal cells by mechanical procedures, (b) selective proliferation of NPCs by addition of bFGF, and (c) induction of midbrain patterning by SHH and FGF8, a largely homogenous population of

NPCs with midbrain marker expressions could be generated from all hiPSCs and hESCs tested. After 6 days of NPC induction of dissociated cells, 92.0% ± 0.4% (Lenti-3) and 86.4% ± 3.1 % (Pro-1) of the total cells were nestin⁺/Ki67⁺ NPCs (Figure 1L). Subpopulations of these NPCs expressed the embryonic midbrain-specific markers Pax2 and/or Pax5 (Figure 1M). mRNA expression of mDA-specific transcription factors (e.g., *LMX1A*, *LMX1B*, engrailed-1 [*EN1*], and *NURR1*) was upregulated during NPC induction and differentiation (Supplemental Figure 2B). Under terminal differentiation conditions after withdrawal of growth factors, hiPSC-derived NPCs (hiPSC-NPCs) predominantly differentiated into TuJ1⁺ neuronal cells (60%–70% of total cells), with a few GFAP⁺ astrocytes (<5%; Figure 1N and Supplemental Figure 3). CNPase⁺ oligodendrocytes were not detected (data not shown), probably because of their late developmental timing. Notably, a major proportion of TuJ1⁺ neuronal cells (35%–45%) was TH⁺ (Figure 1O and Supplemental Figure 3). The next major neuronal subtype was serotonin⁺ neurons (5%–10%; Figure 1P and Supplemental Figure 3). We also observed minor populations of GABAergic or glutamatergic neuronal cells (Supplemental Figure 3 and data not shown).

Residual expression of exogenous reprogramming genes in differentiated cells. An important concern regarding the clinical application of hiPSCs is the potential residual expression and/or reactivation of exogenous reprogramming genes, some of which are related to oncogenesis pathways (23). Residual reprogramming gene expression may also alter or block terminal differentiation of hiPSCs into certain cell lineages. To investigate these issues, we examined Oct4 expression in NPCs and neuronal cells derived from hiPSCs. Strikingly, Oct4 expression was clearly detected in NPCs derived from all 4 lentivirus-based hiPSCs (Figure 2A), although it was much weaker than that in undifferentiated hiPSCs, as examined by immunoreactivity (Supplemental Figure 4, A–C) and mRNA expression (Figure 2D and Supplemental Figure 4D). In addition, Oct4 immunoreactivity was detected in subpopulations of TuJ1⁺ neuronal cells and TH⁺ DA neurons derived from lentivirus-based hiPSCs (Figure 2B). Furthermore, we found that Oct4 expression was significantly upregulated by cAMP treatment (Figure 2C), which indicates that certain signals

Table 2

hESC lines used

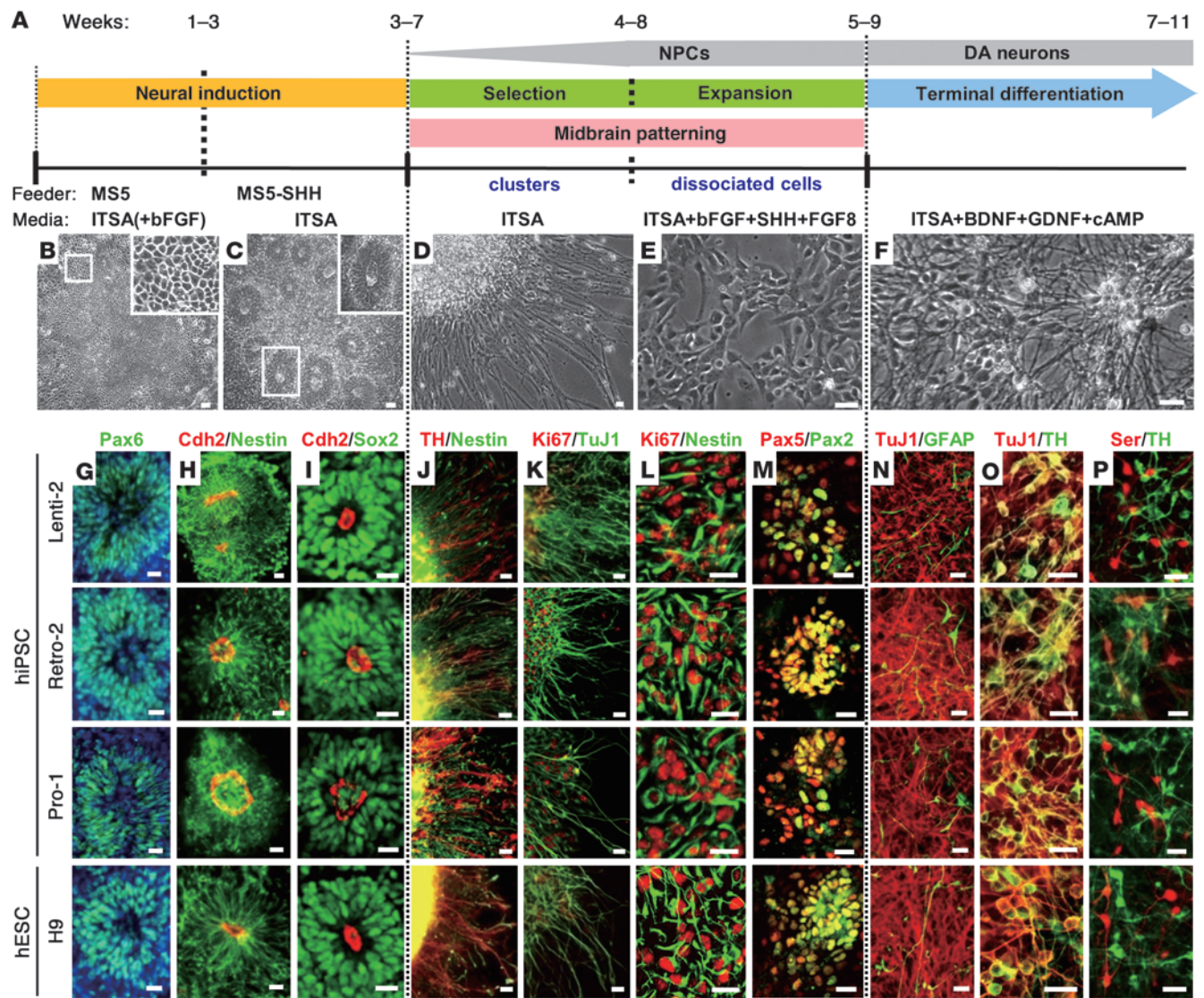| Name	Karyotype	Establishing institute	Reference
HSF-6 (UC06)	Female (46, XX)	UCSF	48
H9 (WA09)	Female (46, XX)	University of Wisconsin	49

Figure 1
Sequential induction of hiPSCs toward NPCs and DA neurons. (**A**) Experimental procedures. (**B–P**) Representative phase-contrast (Pro-1; **B–F**) and immunostaining (**G–P**) images during in vitro differentiation. 2 hESC and 8 hiPSC lines were cocultured on MS5 feeder cells, then subcultured on MS5-SHH. Undifferentiated hiPSC colonies were sequentially transformed into those assembled with small and compactly arranged cells (**B**) and then primitive neuroepithelial rosette structures (**C**) abundantly expressing neural lineage markers such as Pax6, nestin, Sox2, and Cdh2 (**G–I**). Boxed regions are shown enlarged in the insets of **B** (×5) and **C** (×2). Primitive neuroepithelial colonies were harvested, then plated on FN-coated dishes. The majority of cells in the clusters were positive for nestin (**J**) and Ki67 (**K**). At the same time, extensive cellular processes emanating from the clusters were positive for TuJ1 (**K**) and TH (**J**), specific to neurons and DA neurons, respectively. To obtain uniform populations of NPCs, clusters were dissociated and cultured in the same media containing SHH, FGF8, and bFGF, resulting in morphologically and phenotypically uniform NPCs (**E** and **L**), some of which expressed embryonic midbrain markers Pax2 and Pax5 (**M**). Upon terminal differentiation, the majority of NPCs differentiated into neuronal cells extending neurites (**F**) and positive for TuJ1 with a few GFAP+ astrocytes (**N**). Among the TuJ1+ neuronal populations, TH+ neurons were the most abundant (**O** and **P**). Ser, serotonin. Image in **G** is merged with the respective DAPI-stained view (blue). Scale bars: 30 μm.

in vitro or in vivo could reactivate these reprogramming genes. In contrast, Oct4 expression was not detected in NPCs or neuronal cells derived from retrovirus- or protein-based hiPSCs (Figure 2A). To address whether residual Oct4 expression in lentivirus-based hiPSCs originated from the endogenous or the exogenous virus-coded gene, we performed RT-PCR analysis using specific primers (Supplemental Table 2). This analysis revealed that during differentiation of lentivirus-based hiPSCs, exogenous *OCT4* gene expression persisted

(as did that of *NANOG* and *SOX2*), even after generating terminally differentiated neurons (Figure 2D). Interestingly, we found that endogenous *OCT4* gene expression completely disappeared during neuronal differentiation of lentivirus-based hiPSCs, along with other ESC/iPSC markers *DNMT3L*, *REX1*, and *GDF3*, which indicates that an appropriate differentiation program is occurring even in the presence of residual exogenous reprogramming gene expression. This is consistent with our results showing that generation of
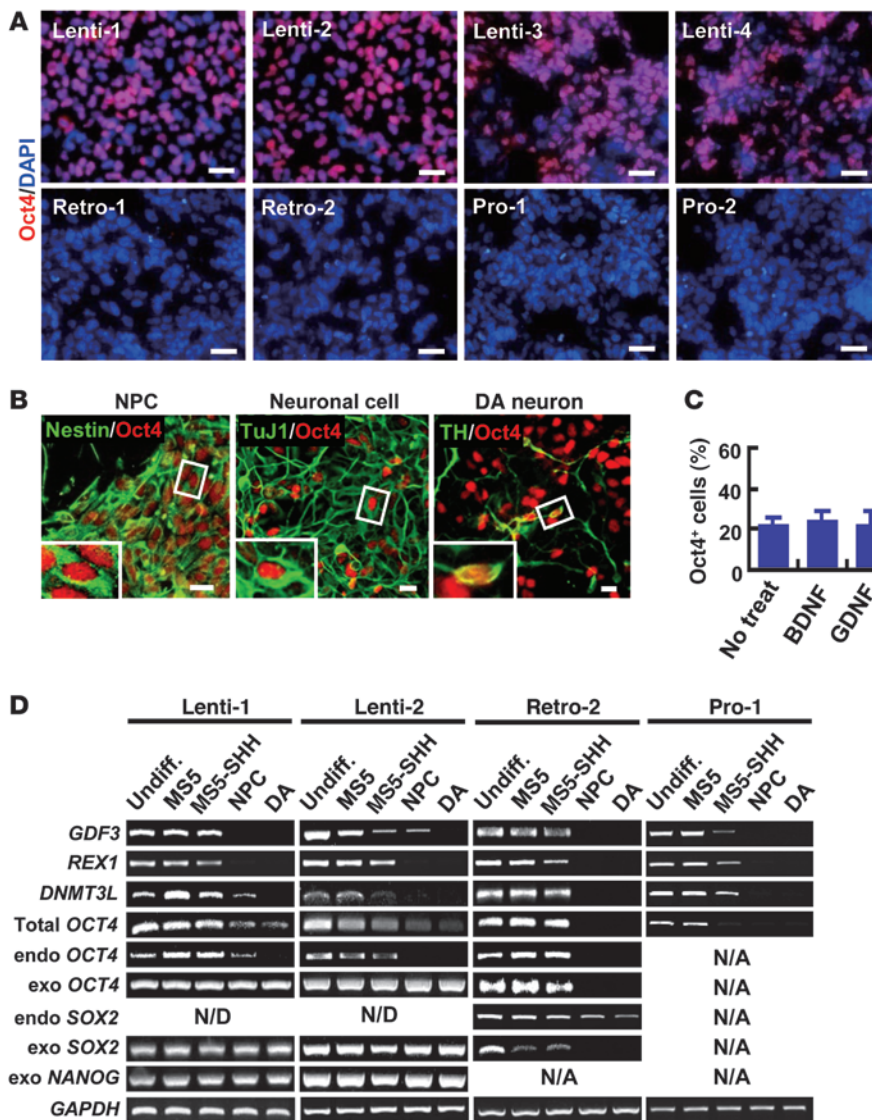
Figure 2
Residual expression of reprogramming genes in differentiated cells from hiPSCs. (**A**) Oct4 expression in hiPSC-NPCs. Substantial Oct4 expression was detected in NPCs derived from all 4 lentivirus-based hiPSCs. (**B**) Oct4 expression was also detected in nestin+ NPCs and in TuJ1+ and TH+ neurons from lentivirus-based hiPSCs before (left) and after (middle and right) terminal differentiation for 7 days. Scale bars: 30 μm. Boxed regions are shown enlarged in the insets (×3). (**C**) Upregulation of Oct4 expression by cAMP treatment. Lenti-3 NPCs were induced to differentiate by withdrawal of bFGF in the absence (No treat) or presence of BDNF, GDNF, or cAMP for 7 days. The percentage of Oct4-positive cells was counted ($n = 4$ coverslips per group). *$P < 0.01$ vs. untreated control, ANOVA with Tukey post-hoc analysis. (**D**) RT-PCR expression analyses for exogenous and endogenous genes. The indicated hiPSCs were cocultured and sequentially differentiated as in Figure 1A. RNAs were prepared from each step: undifferentiated, coculture with MS5, MS5-SHH, NPCs, and differentiated neurons (DA). Primers specific for exogenous (exo; proviral) and endogenous (endo; chromosomal) expression were used. *GDF3*, *REX1*, and *DNMT3L* were used as undifferentiated markers. N/D, not determined; N/A, not applicable (*NANOG* was not used for establishing the retrovirus-based iPSCs).

NPCs, neuronal cells, and DA neurons from lentivirus-based hiPSCs was comparable to that of retrovirus- and protein-based hiPSCs (Figure 1). To examine reprogramming gene expression more quantitatively, we performed real-time PCR analyses for *OCT4* and *NANOG* genes (Supplemental Figure 5). Unlike endogenous gene expression being silenced during neuronal differentiation, expression levels of exogenous reprogramming factor genes in lentivirus-based hiPSCs were not silenced, but rather increased during neuronal differentiation (Supplemental Figure 5, C and F). Based on upregulation of exogenous gene expression by cAMP (Figure 2C), a possible explanation is that the presence of bFGF (which is known to activate the cAMP signaling pathway) and cAMP during NPC and DA neuronal differentiation, respectively, contributed to this increased exogenous reprogramming gene expression. However, it was noted that total levels of *OCT4* and *NANOG* expression significantly diminished during neuronal differentiation (Supplemental Figure 5, A and D), which strongly suggests that the levels of exogenous gene expression represent a minor fraction of the total gene expression levels. It was previously reported that constitutive *SOX2* overexpression inhibits neuronal differentiation (24), raising the interesting question of how efficient neuronal differentiation could occur despite residual *SOX2* expression. Although more detailed analyses are warranted to address this question at the cellular and molecular levels, it is possible that remaining NPCs among differentiated cells contributed, at least in part, to the observed residual *SOX2* expression. In support of this is the prominent expression of Sox2 in NPCs derived from either ESCs/iPSCs (Figure 1I and ref. 25) or developing brains (26). As expected, expression of exogenous reprogramming genes was not detected at any stage of protein-based hiPSC differentiation.

Expansion and senescence of hiPSC-NPCs. We previously showed that mouse (27) and human (17, 28) ESC-derived NPCs are highly expandable and maintain differentiation potentials, in contrast to NPCs from embryonic brain. This proliferative capacity of NPCs is important for the development of cell therapy as well as other applications, such as disease mechanism studies and drug screening platforms. Like hESC-derived NPCs, NPCs from protein-based hiPSCs were stably expandable for at least 8 passages without any change in proliferation index, as examined by total cell number and population doubling level (PDL; Figure 3, A and B). PDLs of Pro-1–derived NPCs were 1.85 at passage 1 (P1) versus 1.50 at P8,
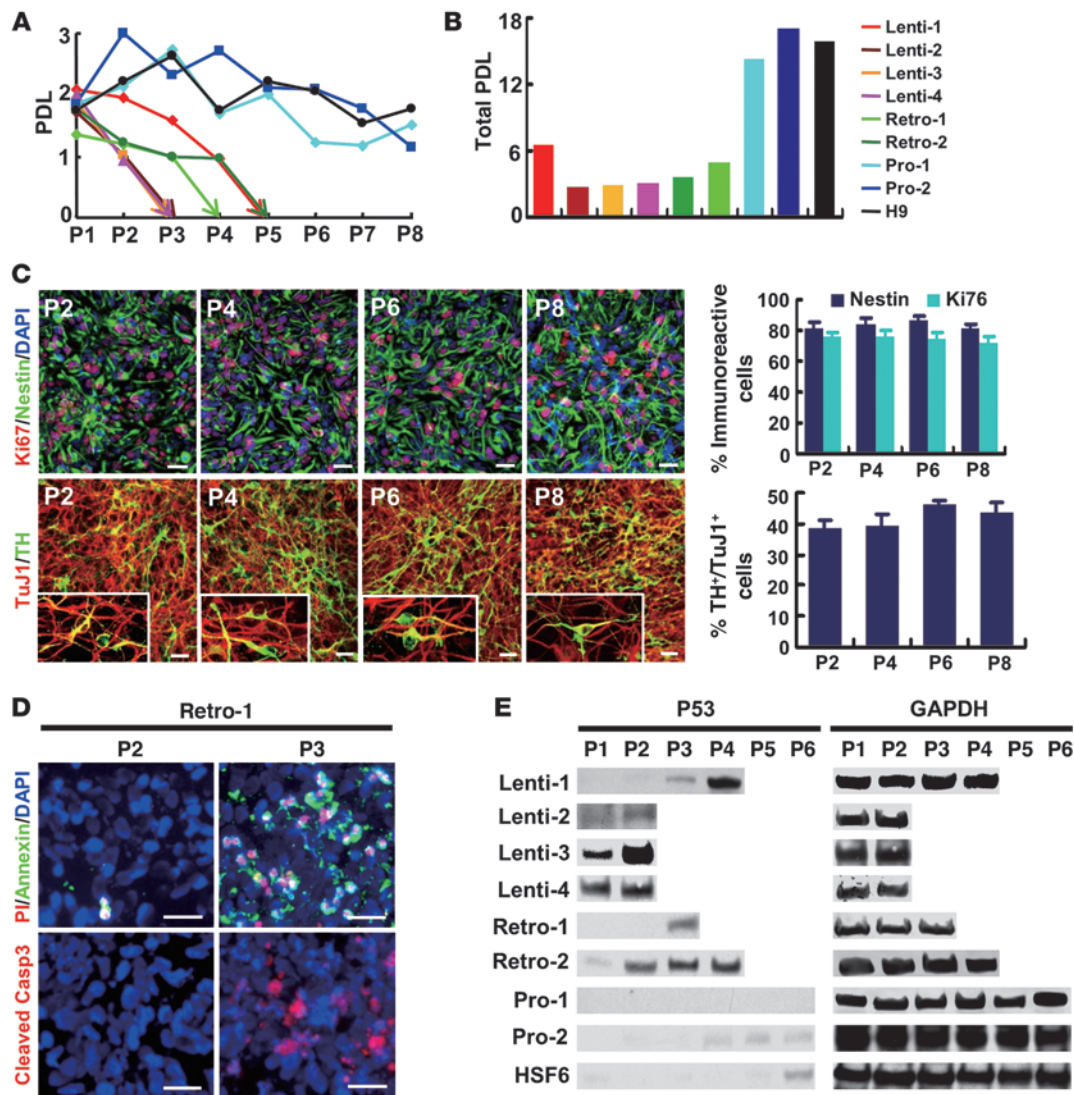
Figure 3
Protein-derived hiPSC-NPCs, but not lentivirus- or retrovirus-based NPCs, are highly expandable without losing their DA neurogenic potentials. NPCs derived from each hiPSC/hESC line were expanded by passaging every 7 days. Cell expansion was estimated by PDL (**A**) and total PDL (**B**), as described in Methods. In **A**, PDL values lower than 0 (in cases when cell numbers on the last day of passages were lower than the initial plating cell number) are indicated by arrows. (**C**) Maintenance of DA neurogenic properties of protein-based hiPSC-NPCs during expansion. Pro-1–derived NPCs were cultured for 8 passages and analyzed by immunochemical analyses for nestin/Ki67 at the last day of each passage. Cells on each passage were differentiated for 15 days and subjected to TH/TuJ1 immunostaining. TH$^+$/TuJ1$^+$ DA neurons are shown enlarged in the insets (×5). Notably, no significant change was observed in percent NPCs (nestin$^+$/Ki67$^+$) after cell expansion or in percent DA neurons (TH$^+$/TuJ1$^+$) after differentiation (n = 3 coverslips per value). P = 0.731–1.000 (nestin$^+$), P = 0.931–1.000 (Ki67$^+$), P = 0.249–0.993 (TH$^+$/TuJ1$^+$), P4, P6, and P8 vs. P2, ANOVA with Scheffe or Tukey post-hoc analysis. (**D** and **E**) Early cell senescence of lentivirus- and retrovirus-based NPCs, with increased apoptotic cell death (**D**) and P53 protein levels (**E**). Shown in **D** is a side-by-side comparison of apoptotic cell markers PI/annexin V and cleaved (activated) caspase 3–immunoreactive cells in P2 and P3 of Retro-1–derived NPC cultures at day 3 of each passage. Scale bars: 30 μm.

and similar numbers of TuJ1$^+$ and TH$^+$ cells were generated from each passage (P2, 38.38% ± 2.54% TH$^+$/TuJ1$^+$; P8, 43.37% ± 3.52% TH$^+$/TuJ1$^+$; n = 3 coverslips per value; Figure 3C). Strikingly, lentivirus-based hiPSC-NPCs abruptly stopped proliferating within 2–4 passages (Figure 3, A and B). Furthermore, retrovirus-based hiPSC-NPCs similarly stopped proliferating within 3–4 passages, which indicates that this early senescence is not the result of residual expression of exogenous reprogramming genes, at least in retrovirus-based hiPSC-NPCs. Dramatic increases of

apoptotic cell death were observed in passaged NPCs from both lentivirus- and retrovirus-based hiPSCs, but not in protein-based hiPSC-NPCs (Figure 3D and data not shown). Since the prototype tumor suppressor P53 critically regulates replicative senescence and apoptosis (29, 30), we hypothesized that its expression/regulation may be altered, leading to early senescence in these virus-based hiPSC-NPCs. Indeed, upregulation/induction of P53 expression preceded cellular senescence of lentivirus- and retrovirus-based NPCs during passaging (Figure 3E).
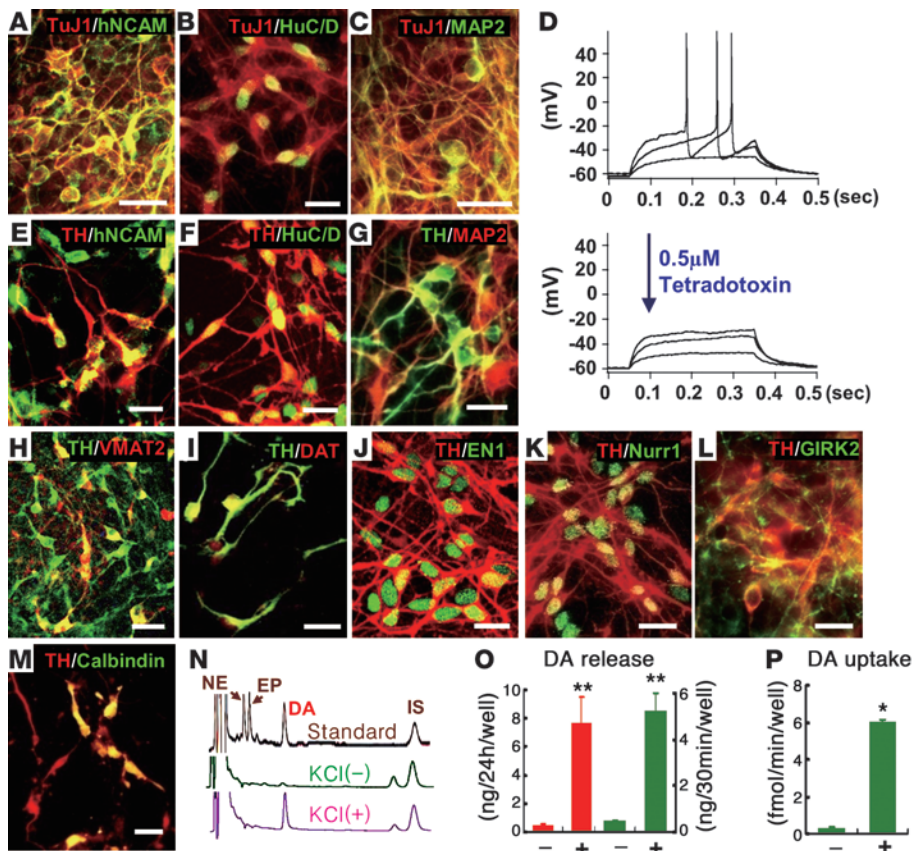
Figure 4
Protein-based hiPSCs generate functional midbrain-like DA neurons in vitro. (**A–C**) TuJ1+ cells differentiated from protein-based hiPSC-NPCs were positive for hNCAM (**A**), HuC/D (**B**), and MAP2 (**C**). (**D**) TuJ1+ cells differentiated from protein-based hiPSC-NPCs were electrophysiologically active neurons. Exemplary membrane potential response upon depolarizing current steps (30, 60, and 90 pA for 300 ms) was abolished by 500 nM tetrodotoxin. (**E–M**) Midbrain marker expression in protein-based hiPSC–derived DA neurons. TH+ cells from differentiated protein-based hiPSC-NPC cultures were immunoreactive for markers specific for neuronal (hNCAM, HuC/D, and MAP2; **E–G**) and for DA homeostasis (VMAT2 and DAT; **H** and **I**). Markers specific for midbrain (EN1 and Nurr1; **J** and **K**), A9 midbrain (GIRK2; **L**), and A10 midbrain (calbindin 1, 28 kDa; **M**) colocalized in subpopulations of TH+ cells. (**N–P**) Presynaptic DA neuronal functions, such as DA release (**N** and **O**) and DA uptake (**P**). (**N**) Typical HPLC chromatograms for DA released in the absence and presence of 56 mM KCl for 30 minutes compared with that of standard mixture (NE, norepinephrine; E, epinephrine). IS, internal standard (3,4-dihydroxybenzylamine) used for quantification of DA concentrations. (**O** and **P**) DA release and uptake values, respectively, of 4 independent cultures. In **P**, DAT-mediated specific DA uptake was calculated by subtracting nonspecific uptake (with nomifensine) from total uptake. *$P < 0.01$, **$P < 0.05$ vs. respective control, 2-tailed Student's *t* test (**O**, left, and **P**) and 2-tailed paired *t* test (**O**, right).

In vitro functional analyses of DA neurons derived from protein-based hiPSCs. Experiments were carried out to determine whether protein-based hiPSCs can efficiently generate functional midbrain-like DA neurons in vitro. As shown in Figure 4, A–C, TuJ1+ cells differentiated from protein-based hiPSC-NPCs exhibited mature neuronal morphologies and expressed mature neuron marker genes (e.g., microtubule-associated protein 2 [MAP2], hNCAM, and HuC/D) at day 15 after differentiation in vitro. Electrophysiological properties of these neuronal cells were examined using standard whole-cell patch techniques. The cells showed high input resistance (2.37 ± 0.57 G ohm), similar to young neurons of hippocampi (31).

Of the 48 cells examined, 39 were able to generate tetrodotoxin-sensitive action potentials in response to depolarizing current injection (Figure 4D), indicative of a Na+ spike, a hallmark feature of differentiated neurons. Importantly, the majority of TH+ cells (>90%) were mature DA neurons, as evidenced by coexpression of neuronal (e.g., hNCAM, HuC/D, and MAP2) and DA markers (vesicular monoamine transporter 2 [VMAT2] and DA transporter [DAT]; Figure 4, E–I). Furthermore, expression of mDA markers (e.g., Nurr1, EN1, the A9 marker potassium inwardly-rectifying channel, subfamily J, member 6 [GirK2]) and the A10 marker calbindin 1, 28 kDa, colocalized in subpopulations of TH+ neurons (Figure 4, J–M). We also tested DA neurotransmitter release and DAT-mediated specific DA reuptake, critical processes in presynaptic mDA neurons. Although DA was minimally detected in Pro-1 NPC cultures before differentiation, it dramatically increased in the culture medium after 15 days of differentiation (Figure 4O). Furthermore, DA release was strikingly evoked by high potassium–induced depolarization stimulus in differentiated cells (basal, 0.49 ± 0.02 ng/30 min/well; evoked by 56 mM KCl, 5.23 ± 0.76 ng/30 min/well; *n* = 4; Figure 4, N and O). In addition, differentiated Pro-1 NPCs exhibited robust DA uptake activities (6.01 ± 0.14 fmol/min/well) compared with those from non–terminally differentiated cultures at the limit of detection (0.27 ± 0.08 fmol/min/well; *n* = 4; Figure 4P). Taken together, our results show that mature midbrain-like functional DA neurons can be efficiently generated from protein-based hiPSCs.

Cell transplantation in PD rats. To examine in vivo function of protein-based hiPSC–derived NPCs and/or DA neurons, transplantation studies were carried out in a well-established rodent model of PD. We used 3 different donor cell conditions for transplantation into the striatum of 6-hydroxydopamine–lesioned rats: condition 1, a high-concentration cell solution of Pro-1 NPCs (3 μl of 2.5×10^5 cells/μl); condition 2, a moderate-concentration cell solution of Pro-1 NPCs (3 μl of 1×10^5 cells/μl); and condition 3, the same moderate number of cells at day 5 of terminal differentiation (3 μl of 1×10^5 cells/μl). As examined by amphetamine-induced rotation scores, condition 1 resulted in a dramatic functional recovery in parkinsonian rats (Figure 5A); at 8 weeks after transplantation, the average rotation score decreased to 23.57% ± 5.48% (*n* = 9) of pretransplantation scores. Notably, 3 of the original 12 grafted animals died as a result of tumor growth before 8 weeks. Abundant
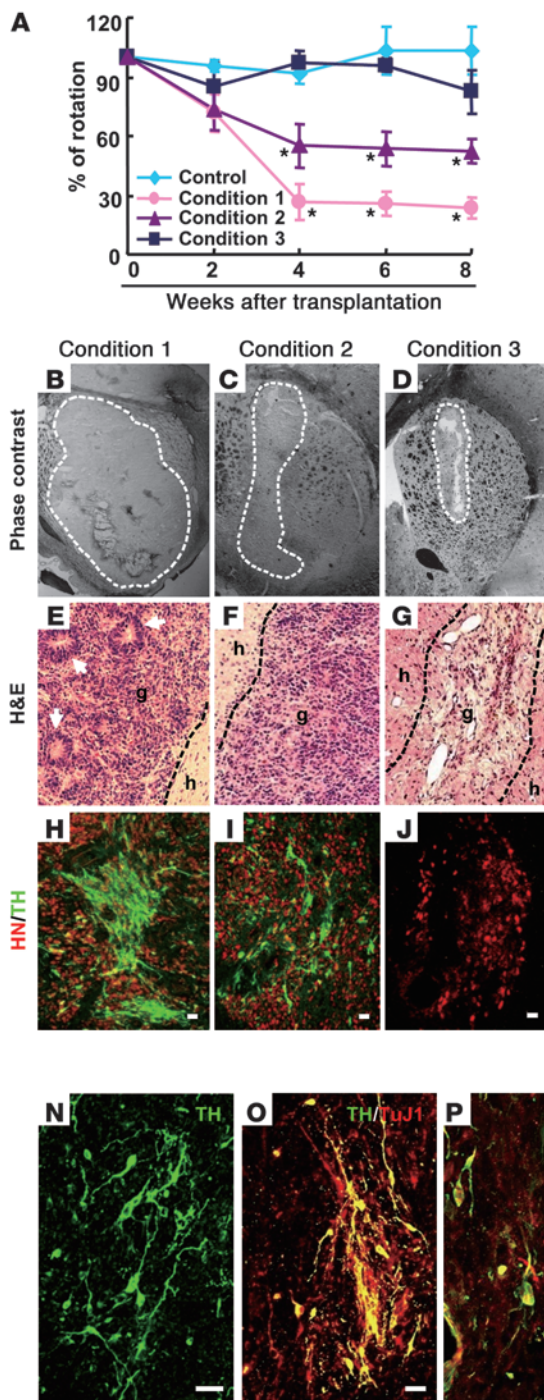
Figure 5
In vivo analyses of protein-based hiPSC-NPCs transplanted to PD model rats. Donor cells were prepared from Pro-1 NPCs and transplanted into 6-hydroxydopamine–lesioned PD rats with 3 different conditions (condition 1, $n = 9$; condition 2, $n = 6$; condition 3, $n = 7$). For the sham control, 6 animals were injected with PBS by the same schedule as the cell-grafted animals. (**A**) Amphetamine-induced rotation scores. Each value depicts mean ± SEM of percent change in score compared with pretransplantation value. *$P < 0.01$ vs. control, ANOVA followed by Scheffe test. (**B–G**) Representative light microscopic (**B–D**; original magnification, ×5) and H&E-stained (**E–G**; original magnification, ×100) views of grafts in the striatum. Dashed lines denote borders between graft (g) and host (h); arrows in **E** indicate neuroepithelial rosettes. (**H–J**) Representative images for TH+/HN+ cells. Tissue sections were initially stained with HN, followed by TH staining with SDS treatment. (**K–M**) Graft volume (**K**), total number of TH+ cells in grafts (**L**), and TH+ cell density in grafts (**M**). (**N–R**) Images for TH+ (**N**), TH+/TuJ1+ (**O**), TH+/VMAT2+ (**P**), TH+/Nurr1+ (**Q**), and TH+/EN1+ (**R**) cells. Images in **H–J** and **N–R** were obtained by stacking z series through the thickness of section (35 μm). Scale bars: 30 μm.

TH+ cells (54,418 ± 23,660 cells/graft; Figure 5L) were observed in the grafted brains of surviving rats 8 weeks after transplantation (Figure 5H). However, these grafts were large (occupying more than half the striatum, 24.57 ± 9.75 mm³; Figure 5, B and K) and contained numerous neuroepithelial rosette structures (Figure 5E) with cells positive for nestin and the proliferating cell markers (Supplemental Figure 6), indicative of robust cell proliferation and remaining immature cells. Under condition 2, a moderate but significant level of functional recovery was observed (e.g., 52.46% ± 6.28% of pretransplant rotation scores at 8 weeks after transplantation;

$n = 6$; Figure 5A), without any graft-related death. The graft size was more appropriate and uniform (4.74 ± 1.94 mm³; Figure 5, C and K), without irregular proliferating mass or rosette formation (Figure 5F). TH+ cells (26,882 ± 9,089 cells/graft) were evenly distributed throughout the grafts (Figure 5, L and I). A majority of TH+ cells coexpressed TuJ1 and VMAT2; moreover, some were positive for Nurr1 and EN1 (Figure 5, N–R). This is in sharp contrast to condition 1, in which the graft size was substantially larger, tumor-related death occasionally occurred, and a huge number of proliferating/undifferentiated cell mass was found. In addition,

TH⁺ cells were not detected in proliferating NPC masses, but were mostly found at the interphase between proliferating/undifferentiated cell clusters, indicative of inefficient NPC differentiation in condition 1. These findings emphasize the importance of optimizing the number and condition of transplanted cells to assure optimal outcomes. Notably, under condition 3, no behavioral recovery was observed, and no TH⁺ cells were readily detectable in the graft (Figure 5, A, J, L, and M). Severe cell death was evident from the central area of the grafts (Figure 5, D and G), which strongly suggested that the differentiation stage is a critical factor for functional outcomes of cell transplantation.

Discussion

Although hiPSCs hold great promise as platforms to study and treat human disorders, it is critical to carefully assess their safety for clinical and biomedical application. In particular, hiPSCs generated using retroviruses and lentiviruses have chromosomal integrations that may lead to unpredictable genetic dysfunction. Our present results demonstrated that there was residual exogenous gene expression even when lentivirus-based hiPSCs were terminally differentiated into NPCs or neurons. In contrast, expression of the reprogramming genes was not readily detected in retrovirus-based hiPSCs after neural differentiation, indicative of almost complete silencing of exogenous genes. At present, it is not known why exogenous reprogramming genes exhibit differential silencing in lentivirus- and retrovirus-based hiPSC lines. Interestingly, during hematopoietic differentiation of mouse ESCs, gene expression from the retrovirus long terminal repeat (LTR), but not from the lentivirus, was severely reduced (32), which appears to be caused by methylation of the retroviral LTR promoter (33). Thus, it is possible that differential promoter methylation underlies the distinct silencing between lentivirus- and retrovirus-based hiPSCs.

Although NPCs derived from retrovirus- and lentivirus-based hiPSCs displayed limited expandability and early senescence, neuronal differentiation appeared to occur normally in all hiPSCs, as evidenced by efficient generation of NPCs and DA neurons under our optimized procedure. These observations suggest that retrovirus- and lentivirus-based hiPSCs may be useful for a variety of biological and neurorepair studies, even if they are an unsuitable source of cells for future personalized medicine. A recent study demonstrated that hiPSCs generated by the lentiviral method exhibit neural differentiation capacity with significantly reduced efficiency and increased variability compared with hESCs (13). We also recently showed that derivative cells (e.g., hemangioblasts, endothelial cells, and hematopoietic cells) could be generated from lentivirus- and retrovirus-derived hiPSC lines with phenotypes similar to those derived from hESCs, but with a dramatic decrease in efficiency (34). In distinct contrast to the hESC derivatives, hemangioblasts derived from virus-based hiPSCs showed significantly increased apoptosis, severely limited expansion capability, and substantially decreased hematopoietic colony-forming capability. Taken together, these results suggest that limited expandability and early senescence of derivative precursor cells is a common phenomenon for lentivirus- and retrovirus-based hiPSCs with genomic disruptions. Interestingly, we found that P53 expression was induced in apoptotic NPCs derived from lentivirus- and retrovirus-based hiPSCs before they underwent massive apoptosis. Why P53 is induced in these cells, but not in NPCs derived from hESCs or protein-based hiPSCs, warrants further investigation.

To overcome the potential caveats associated with residual exogenous reprogramming genes and chromosomal integrations, several groups have recently reported new approaches of hiPSC generation, including use of minimal numbers of reprogramming genes (35), use of small molecules (36, 37), excision of the remaining transgenes (38–40), and use of nonintegrating vectors (41, 42). It will be important to determine whether these hiPSCs behave similarly to hESCs and protein-based hiPSCs in terms of differentiation and function of their derivative progenitor cells.

To our knowledge, this is the first study to directly compare the differentiation and cellular properties of hiPSCs generated by chromosome integrating and nonintegrating methods. A potential limitation of this work is that we used disparate hiPSC lines derived from different cell sources, at different passages, and handled by different laboratories, any of which can substantially affect the properties of individual hiPSC lines. Thus, a more straightforward comparison could be made using individual hiPSC lines generated from the same cell source via different reprogramming methods and used at similar passage and culture conditions. Despite these possible limitations, our data demonstrate fundamental and consistent differences in cellular and differentiation properties within each group of hiPSC lines without any exception, which strongly supports that these results are not due to experimental artifacts. Thus, our results suggest that protein-based hiPSCs may serve as a promising source of cells for clinical translation. These cells behaved similar to hESCs without abnormal senescence/apoptosis, they did not show any exogenous reprogramming gene expression, and DA neurons derived from protein-based hiPSCs significantly improved behavioral defects in a rodent model of PD. A high number of TH⁺ neurons (>25,000 cells/graft) survived over months after transplantation with prominent behavioral effect. This is in clear contrast to most hESC/hiPSC transplantation studies, which show only modest behavioral improvements in rodent PD models with much fewer surviving TH⁺ neurons (e.g., refs. 43, 44). Although it is not clear whether these differences are related to the hiPSC lines used in the present studies and how they were derived, it is likely that our optimized differentiation protocol and/or the stage of cell transplantation contributed to the different functional outcomes. In line with this, no functional recovery was observed when we transplanted the differentiated cells. Although tumorigenic masses were observed when a large number of cells was transplanted, this was most likely caused by the remaining undifferentiated cells. This underscores the importance of establishing clinically safe methods for complete removal of undifferentiated cells, as evidenced by a recent comprehensive study of multiple mouse iPSC lines showing the correlation of teratoma-forming propensities and remaining undifferentiated cells (12). Our results suggest that protein-based reprogramming may be a viable approach for generating a patient-specific source of cells for treatment of PD and other degenerative diseases.

Methods

Study approval. Studies using hESCs and hiPSCs were approved by the IRB at Hanyang University and by the Partners Human Embryonic Stem Cell Research Oversight (ESCRO) Committee (protocol no. 2006-06-01). The IACUC of Hanyang University College of Medicine approved all protocols for animal care and treatment in this study.

Differentiation of hiPSCs and hESCs. The hiPSCs and hESCs used in this study are listed in Tables 1 and 2. Undifferentiated hiPSCs and hESCs were propagated on MEF feeder and differentiated toward midbrain-type

NPCs on feeder layers of MS5 and subsequently on MS5-SHH as previously described (17, 45). bFGF (20 ng/ml) was supplemented during the first week of the coculture period. Neuroepithelial cell colonies were transferred onto polyornithine/FN-coated dishes and cultured for the proliferation and midbrain patterning of NPCs for 7 days in ITS media plus AA (ITSA; 200 μmol/l) supplemented with bFGF (20 ng/ml), SHH (200 μg/ml), and FGF8 (100 μg/ml; R&D Systems). The expanded cell clusters were dissociated into single cells after incubating in Ca^{+2}/Mg^{+2}-free Hanks balanced salt solution for 30 minutes, and subcultured in the same expansion medium (NPC P1). The NPCs were subcultured every 7 days. Terminal differentiation of hiPSC- and hESC-derived NPCs was induced in ITSA supplemented with dibutyryl cAMP (0.5 mmol/ml; Sigma-Aldrich), brain-derived neurotrophic factor (BDNF; 20 ng/ml), and glial cell line–derived neurotrophic factor (GDNF; 20 ng/ml; R&D Systems). The NPCs at every passage were stored in liquid N_2 and recultured when required.

Immunofluorescent staining. Cultured cells or cryosectioned brain slices were fixed with 4% paraformaldehyde in PBS and incubated overnight at 4°C with primary antibodies listed in Supplemental Table 1. Appropriate fluorescence-tagged secondary antibodies (Jackson Immunoresearch Laboratories) were used for visualization. Stained samples were mounted in VECTASHIELD with DAPI mounting medium (Vector Laboratories) and photographed using epifluorescence and confocal microscope (Leica). Measurement of fluorescence intensity was computed with the Leica Application Suite (LAS) image analysis package.

Semiquantitative and quantitative RT-PCR. Total RNA preparation, cDNA synthesis, and RT-PCR reactions were performed as described previously (45). Real-time PCR was performed on a CFX96 Real time system using iQ SYBR green supermix (Bio-Rad). Gene expression values were normalized to those of *GAPDH*. See Supplemental Table 2 for primers.

Measurement of cell expansion. NPCs derived from each hiPSC and hESC line were expanded for 56 days by passaging every 7 days (total 8 passages). Cell expansion of each NPC passage was estimated by PDL, calculated as $\log_{N/No}/\log_2$, where N is the number of cells at the end of each passage and No is the number of cells plated initially (2.5×10^5 cells/cm²). Cumulative (total) PDL is the sum of individual PDLs up to NPC P8. For NPC cultures in which cell growth stopped earlier than P8 (Lenti-1–Lenti-4, Retro-1, and Retro-2), the cumulative PDL values are the sum of PDLs during sustained cell growth (PDL > 0).

Apoptotic cell detection by annexin V and propidium iodide. Apoptotic cells were labeled with annexin V–FITC and propidium iodide using the annexin V–FLUOS staining kit (Roche) according to the manufacturer's instructions.

Western blot analyses. Cell lysis and immunoblotting were done as previously described (46). Proteins were extracted in lysis buffer, subjected to denaturing sodium dodecyl sulfate polyacrylamide gel electrophoresis, and transferred to a nitrocellulose membrane. Transferred proteins were blocked in 5% nonfat milk in 0.001% Tween 20 with Tris-buffered saline. The blot was probed with anti-mouse P53 (1:1,000 dilution; Cell Signaling) followed by treatment with anti-mouse IgG antibodies conjugated with peroxidase (1:2,000 dilution; Cell Signaling). Bands were visualized by enhanced chemiluminescence (Welgene).

Electrophysiology. Whole-cell patch recordings were made at 30°C with an EPC10/2 amplifier (HEKA). The bathing solution contained 124 mM NaCl, 26 mM $NaHCO_3$, 3.2 mM KCl, 2.5 mM $CaCl_2$, 1.3 mM $MgCl_2$, 1.25 mM $NaHPO_4$, and 10 mM glucose and saturated with 95% O_2 and 5% CO_2. The pipette (3–4 MΩ) solution for whole-cell patch clamp contained 140 mM K-gluconate, 5 mM di-Tris-phosphocreatin, 5 mM NaCl, 4 mM MgATP, 0.4 mM Na_2GTP, 15 mM HEPES, and 2.5 mM Na pyruvate at pH 7.3 (adjusted with KOH).

DA uptake assay. DA uptake in intact cells was conducted as described previously (45). Briefly, experiments were carried out at 37°C for 10 minutes using 50 nmol/l [³H]DA (51 Ci/mmol; Amersham Co.) with or without 10 μmol/l nomifensine (RBI), a DAT blocker, to determine nonspecific uptake. After incubation, uptake reactions were terminated by aspiration of the reaction solution and washing twice with ice-cold PBS. Cells were lysed with 0.5 mol/l NaOH, and the radioactivity was measured by liquid scintillation counting (Perkin Elmer). Specific DA uptake was calculated by subtracting nonspecific uptake (with 10 μM nomifensine) from the uptake value without nomifensine.

DA release by HPLC. HPLC analysis to determine DA levels was performed as previously described (17). To determine DA released from differentiated precursor cells with or without terminal differentiation, ITSA media conditioned in the cells for 24 hours were collected. DA release evoked by depolarization was also determined in terminally differentiated cells. Cells at terminal differentiation day 15 were incubated in ITSA with (evoked) or without (basal release) 56 mmol/l KCl for 30 minutes, and the media were collected. The collected medium was stabilized with 0.1 N perchloric acid containing 0.1 mmol/l EDTA, followed by extraction by aluminum adsorption. DA was separated on a reverse-phase l-Bondapak C18 column (150 · 3.0 mm; Eicom) at a flow rate of 0.5 ml/min. Electroactive compounds were analyzed at +750 mV using an analytical cell and an amperometric detector (Model ECD-300; Eicom). DA levels were calculated using an internal standard (50 nmol/l methyl-DOPA) and catecholamine standard mixtures, including 1–50 nmol/l DA (external standard) injected immediately before and after each experiment.

In vivo transplantation and histological procedure. The generation of 6-hydroxydopamine–lesioned PD model rats and the amphetamine-induced rotation test were performed as described previously (17). For transplantation, 3 different conditions for the preparation of Pro-1 NPCs were used (condition 1, NPC P1–P2, 2.5×10^5 cells/μl, 3 μl; condition 2, NPC P4, 1×10^5 cells/μl, 3 μl; condition 3, predifferentiated NPCs, 1×10^5 cells/μl, 3 μl). Dissociated Pro-1 NPCs were injected over a 5-minute period into each of 2 sites of the striatum (coordinates in AP, ML, and V relative to bregma and dura: [a] 0.07, –0.30, –0.55; [b] –0.10, –0.40, –0.50; incisor bar set at 3.5 mm below 0) under anesthesia induced by ketamine (4.5 mg/kg) mixed with Rompun (93.28 μg/kg). The needle (22 gauge) was left in place for 5 minutes after completion of each injection. Rats received daily injections of cyclosporine A (10 mg/kg i.p.) starting 1 day before grafting and continuing for 8 weeks thereafter. 8 weeks after transplantation, animals were anesthetized (50 mg/kg pentobarbital) and perfused intracardially with 4% paraformaldehyde. Brains were removed and immersed in 30% sucrose in PBS overnight, frozen in Tissue-Tek (Sakura Finetek USA), and then sliced on a freezing microtome (Leica). Free-floating brain sections (30 μm thick) were subjected to immunohistochemistry as described above, and images were obtained with a confocal microscope (Leica). The total number of cells positive for TH in the graft was counted. To compensate for double counting in adjacent sections, Abercrombie correction factor ($N = n \times T/[T + D]$; where N is the actual number of cells, n is the number of nuclear profiles, T is the section thickness, and D is the average diameter of nuclei) was used. Graft areas were determined using LAS image analysis, and the Cavalieri estimator was used to calculate graft volumes.

Cell counting. Immunoreactive cells on coverslip cultures were counted on randomly selected microscopic fields in a region of uniform cell growth using an eyepiece grid at a final magnification of ×200 or ×400. On each coverslip, 10–20 microscopic fields were counted, and 2–3 coverslips were analyzed in each experimental group.

Statistics. Data are expressed as mean ± SEM of at least 3 independent experiments. Statistical comparisons were made by Student's 2-tailed t test and 2-tailed paired t test, ANOVA, with Scheffe or Tukey post-hoc analysis (SPSS 15.0) when 2 or more groups were involved. The 2-tailed paired t test was applied for comparison of HPLC with or without KCl.

Address correspondence to: Sang-Hun Lee, Department of Biochemistry and Molecular Biology, College of Medicine, Hanyang University, 17 Haengdang-dong, Sungdong-gu, Seoul 133-791, Republic of Korea. Phone: 82.2.2220.0625; Fax: 82.2.2294.6270; E-mail: leesh@hanyang.ac.kr. Or to: Kwang-Soo Kim, Molecular Neurobiology Laboratory, McLean Hospital, 115 Mill St., Belmont, Massachusetts 02478, USA. Phone: 617.855.2024; Fax: 617.855.2220; E-mail: kskim@mclean.harvard.edu.

Wonhee Suh's present address is: College of Pharmacy, Ajou University, Seoul, Republic of Korea.

1. Savitt JM, Dawson VL, Dawson TM. Diagnosis and treatment of Parkinson disease: molecules to medicine. *J Clin Invest*. 2006;116(7):1744–1754.
2. Piccini P, et al. Dopamine release from nigral transplants visualized in vivo in a Parkinson's patient. *Nat Neurosci*. 1999;2(12):1137–1140.
3. Freed CR, et al. Transplantation of embryonic dopamine neurons for severe Parkinson's disease. *N Engl J Med*. 2001;344(10):710–719.
4. Dunnett SB, Bjorklund A, Lindvall O. Cell therapy in Parkinson's disease - stop or go? *Nat Rev Neurosci*. 2001;2(5):365–369.
5. Takahashi K, Yamanaka S. Induction of pluripotent stem cells from mouse embryonic and adult fibroblast cultures by defined factors. *Cell*. 2006;126(4):663–676.
6. Takahashi K, et al. Induction of pluripotent stem cells from adult human fibroblasts by defined factors. *Cell*. 2007;131(5):861–872.
7. Yu J, et al. Induced pluripotent stem cell lines derived from human somatic cells. *Science*. 2007;318(5858):1917–1920.
8. Park IH, et al. Reprogramming of human somatic cells to pluripotency with defined factors. *Nature*. 2008;451(7175):141–146.
9. Gearhart J, Pashos EE, Prasad MK. Pluripotency redux--advances in stem-cell research. *N Engl J Med*. 2007;357(15):1469–1472.
10. Kim D, et al. Generation of human induced pluripotent stem cells by direct delivery of reprogramming proteins. *Cell Stem Cell*. 2009;4(6):472–476.
11. Osafune K, et al. Marked differences in differentiation propensity among human embryonic stem cell lines. *Nat Biotechnol*. 2008;26(3):313–315.
12. Miura K, et al. Variation in the safety of induced pluripotent stem cell lines. *Nat Biotechnol*. 2009;27(8):743–745.
13. Hu BY, et al. Neural differentiation of human induced pluripotent stem cells follows developmental principles but with variable potency. *Proc Natl Acad Sci U S A*. 2010;107(9):4335–4340.
14. Kawasaki H, et al. Induction of midbrain dopaminergic neurons from ES cells by stromal cell-derived inducing activity. *Neuron*. 2000;28(1):31–40.
15. Perrier AL, et al. Derivation of midbrain dopamine neurons from human embryonic stem cells. *Proc Natl Acad Sci U S A*. 2004;101(34):12543–12548.
16. Kim DW, et al. Stromal cell-derived inducing activity, Nurr1, and signaling molecules synergistically induce dopaminergic neurons from mouse embryonic stem cells. *Stem Cells*. 2006;24(3):557–567.
17. Ko JY, et al. Human embryonic stem cell-derived neural precursors as a continuous, stable, and on-demand source for human dopamine neurons. *J Neurochem*. 2007;103(4):1417–1429.
18. Shen Q, et al. Endothelial cells stimulate self-renewal and expand neurogenesis of neural stem cells. *Science*. 2004;304(5675):1338–1340.
19. Roy NS, Cleren C, Singh SK, Yang L, Beal MF, Goldman SA. Functional engraftment of human ES cell-derived dopaminergic neurons enriched by coculture with telomerase-immortalized midbrain astrocytes. *Nat Med*. 2006;12(11):1259–1268.
20. Pankratz MT, Li XJ, Lavaute TM, Lyons EA, Chen X, Zhang SC. Directed neural differentiation of human embryonic stem cells via an obligated primitive anterior stage. *Stem Cells*. 2007;25(6):1511–1520.
21. Elkabetz Y, Panagiotakos G, Al Shamy G, Socci ND, Tabar V, Studer L. Human ES cell-derived neural rosettes reveal a functionally distinct early neural stem cell stage. *Genes Dev*. 2008;22(2):152–165.
22. LaVaute TM, Yoo YD, Pankratz MT, Weick JP, Gerstner JR, Zhang SC. Regulation of neural specification from human embryonic stem cells by BMP and FGF. *Stem Cells*. 2009;27(8):1741–1749.
23. Okita K, Nakagawa M, Hyenjong H, Ichisaka T, Yamanaka S. Generation of mouse induced pluripotent stem cells without viral vectors. *Science*. 2008;322(5903):949–953.
24. Graham V, Khudyakov J, Ellis P, Pevny L. SOX2 functions to maintain neural progenitor identity. *Neuron*. 2003;39(5):749–765.
25. Kim JB, et al. Pluripotent stem cells induced from adult neural stem cells by reprogramming with two factors. *Nature*. 2008;454(7204):646–650.
26. Favaro R, et al. Hippocampal development and neural stem cell maintenance require Sox2-dependent regulation of Shh. *Nat Neurosci*. 2009;12(10):1248–1256.
27. Chung S, et al. Neural precursors derived from embryonic stem cells, but not those from fetal ventral mesencephalon, maintain the potential to differentiate into dopaminergic neurons after expansion in vitro. *Stem Cells*. 2006;24(6):1583–1593.
28. Hong S, Kang UJ, Isacson O, Kim KS. Neural precursors derived from human embryonic stem cells maintain long-term proliferation without losing the potential to differentiate into all three neural lineages, including dopaminergic neurons. *J Neurochem*. 2008;104(2):316–324.
29. Sharpless NE, DePinho RA. How stem cells age and why this makes us grow old. *Nat Rev Mol Cell Biol*. 2007;8(9):703–713.
30. Green DR, Kroemer G. Cytoplasmic functions of the tumour suppressor p53. *Nature*. 2009;458(7242):1127–1130.
31. Lee SH, Ho WK. Characterization of somatic Ca2+ clearance mechanisms in young and mature hippocampal granule cells. *Cell Calcium*. 2009;45(5):465–473.
32. Hamaguchi I, et al. Lentivirus vector gene expression during ES cell-derived hematopoietic development in vitro. *J Virol*. 2000;74(22):10778–10784.
33. Laker C, et al. Host cis-mediated extinction of a retrovirus permissive for expression in embryonal stem cells during differentiation. *J Virol*. 1998;72(1):339–348.
34. Feng Q, et al. Hemangioblastic derivatives from human induced pluripotent stem cells exhibit limited expansion and early senescence. *Stem Cells*. 2010;28(4):704–712.
35. Kim JB, et al. Direct reprogramming of human neural stem cells by OCT4. *Nature*. 2009;461(7264):649–643.
36. Borowiak M, et al. Small molecules efficiently direct endodermal differentiation of mouse and human embryonic stem cells. *Cell Stem Cell*. 2009;4(4):348–358.
37. Lin T, et al. A chemical platform for improved induction of human iPSCs. *Nat Methods*. 2009;6(11):805–808.
38. Soldner F, et al. Parkinson's disease patient-derived induced pluripotent stem cells free of viral reprogramming factors. *Cell*. 2009;136(5):964–977.
39. Woltjen K, et al. piggyBac transposition reprograms fibroblasts to induced pluripotent stem cells. *Nature*. 2009;458(7239):766–770.
40. Kaji K, Norrby K, Paca A, Mileikovsky M, Mohseni P, Woltjen K. Virus-free induction of pluripotency and subsequent excision of reprogramming factors. *Nature*. 2009;458(7239):771–775.
41. Yu J, et al. Human induced pluripotent stem cells free of vector and transgene sequences. *Science*. 2009;324(5928):797–801.
42. Jia F, et al. A nonviral minicircle vector for deriving human iPS cells. *Nat Methods*. 2010;7(3):197–199.
43. Hargus G, et al. Differentiated Parkinson patient-derived induced pluripotent stem cells grow in the adult rodent brain and reduce motor asymmetry in Parkinsonian rats. *Proc Natl Acad Sci U S A*. 2010;107(36):15921–15926.
44. Swistowski A, et al. Efficient generation of functional dopaminergic neurons from human induced pluripotent stem cells under defined conditions. *Stem Cells*. 2010;28(10):1893–1904.
45. Park CH, et al. In vitro and in vivo analyses of human embryonic stem cell-derived dopamine neurons. *J Neurochem*. 2005;92(5):1265–1276.
46. Jo AY, et al. Generation of dopamine neurons with improved cell survival and phenotype maintenance using a degradation-resistant nurr1 mutant. *Stem Cells*. 2009;27(9):2238–2246.
47. Lee TH, et al. Functional recapitulation of smooth muscle cells via induced pluripotent stem cells from human aortic smooth muscle cells. *Circ Res*. 2010;106(1):120–128.
48. Carpenter MK, Rosler E, Rao M. Characterization and differentiation of human embryonic stem cells. *Cloning Stem Cells*. 2003;5(1):79–88.
49. Thomson JA, et al. Embryonic stem cell lines derived from human blastocysts. *Science*. 1998;282(5391):1145–1147.